Heavy-quark potential in the Gribov-Zwanziger approach around the deconfinement phase transition

Wan Wu, Guojun Huang, Jiaxing Zhao, and Pengfei Zhuang
Physics Department, Tsinghua University, Beijing 100084, China

(Received 19 July 2022; accepted 9 June 2023; published 27 June 2023)

The interaction potential between a pair of heavy quarks is calculated with the resummed perturbation method in Gribov-Zwanziger (GZ) approach around the deconfinement phase transition. The resummed loop correction makes the potential complex. While the real part is suppressed by color screening and becomes short-ranged at high temperatures, the imaginary part is enhanced through decay processes in a hot medium and becomes comparable with the real part around the phase transition. The strong imaginary potential comes from the magnetic scale in the GZ approach and shows that both the color screening and decay processes play important roles in quarkonium dissociation in high-energy nuclear collisions.

DOI: 10.1103/PhysRevD.107.114033

Considering the large mass m and small velocity v, there exists a hierarchy of energy scales $m \gg mv \gg mv^2$ for heavy quarks. When integrating out the momentum larger than m and mv from the Quantum Chromodynamics (QCD) respectively, one obtains the nonrelativistic QCD (NRQCD) and potential nonrelativistic QCD (pNRQCD) theories [1–3] for the study of heavy quark systems. At the leading order, the equation of motion in pNRQCD returns to the Schrödinger equation in quantum mechanics, and the dynamics are fully described by an interaction potential. The two-body Schrödinger equation with the Cornell potential between a pair of heavy quarks successfully describes the quarkonium properties in vacuum [4]. The one-gluon exchange between two heavy quarks gives rise to the Coulomb part of the potential, while the confinement part should come from nonperturbative calculations through for instance lattice simulations [5,6].

In recent years heavy-flavor hadrons are widely considered as a probe of the new state of matter—quark-gluon plasma (QGP) created in relativistic heavy-ion collisions [4,7–14]. This extends the study of heavy-quark potential from vacuum to finite temperature. In a hot medium of light quarks and gluons, the heavy-quark potential is expected to become complex: The color screening by the surrounding quarks and gluons reduces the Cornell potential [15–18], an analogy to the Debye screening in electromagnetic systems, and the imaginary part is introduced by the Landau damping or color singlet-to-octet transition [19]. The potential can be extracted from the quarkonium spectra via lattice QCD simulations [20–25]. Recently, the machine learning method [26] and some spectral extraction strategies [27,28] are used to obtain the potential, indicating a large imaginary part.

At extremely high temperatures, the Landau damping becomes dominant, and the potential can be well described by the Hard-Thermal-Loop (HTL) resummed perturbation [29,30]. However, the perturbation calculation shows poor convergence at lower temperatures $T \leq 2T_c$ with T_c being the QCD phase transition temperature. This weak convergence appears also in the calculation of QCD thermodynamics, attributed to the IR sector of QCD [31]. The electric Debye mass can not remove all the infrared divergences of QCD unless introducing a magnetic mass which is at the order of g^2T [31,32]. The magnetic mass enters only in higher-order calculations, and its contribution is significant at low temperatures where the coupling constant g is large.

In QCD ghosts are required by the gauge fixing in non-Abelian theory [33]. In 1978 Gribov discovered that the gauge fixing in the quantization is not complete, there exist still gauge copies that could affect the infrared region of those gauge quantities such as the gluon and ghost propagators [34]. The Gribov action arises from the restriction of the domain of the integration in Euclidean space to the Gribov region Ω, which is defined as the set of all gauge field configurations fulfilling a gauge (for instance the Landau gauge $\partial^\mu A^a_\mu = 0$) and for which the Faddeev-Popov operator $M^{ab} = -\partial_\mu(\delta^{ab}\partial^\mu - gf^{abc}A^\mu_c)$ is strictly positive [34,35]. The original Gribov Lagrangian includes a nonlocal term and is hard to calculate. Zwanziger used the BRST method [36–38] to modify the Lagrangian through the introduction of a set of auxiliary fields and derived the Gribov-Zwanziger (GZ) Lagrangian in a local form which is now used widely [39–42]. The GZ approach is further revised by considering the gluon condensate and

including some mass terms in the Lagrangian [43]. From the original GZ approach, one can read off the gluon propagator. For instance, in the Landau gauge [34] it is

$$D^{ab}_{\mu\nu}(p) = \delta^{ab}\left(\delta_{\mu\nu} - \frac{p_\mu p_\nu}{p^2}\right)\frac{p^2}{p^4 + m_G^4}, \tag{1}$$

where m_G is the Gribov mass parameter. In comparison with the normal gluon propagator in the limit of $m_G \to 0$, the GZ propagator has complex poles at $p^2 = \pm i m_G^2$ and is suppressed in the infrared region. This structure does not allow us to attach the usual particle meaning to the gluon propagator, invalidating the interpretation of gluons as an excitation of the physical spectrum. Gluons are confined by the Gribov condition. The Gribov mass parameter $m_G \sim g^2 T$ [39] at high temperature is proportional to the magnetic mass. Therefore, the magnetic scale is automatically incorporated into the framework of the GZ approach. The QCD thermodynamic quantities are investigated in the GZ approach and consistent with the lattice data [42,44]. In the following calculation, we choose the Coulomb gauge; the corresponding gluon propagator can be found in Ref. [45].

Because the confinement is already reflected in the gluon propagator (1) at the lowest order, the GZ approach provides a possibility to perturbatively calculate the heavy-quark potential. This can provide a way to understand the physics of the complex potential extracted from the lattice data. The calculation at the one-loop level in vacuum shows a Coulomb potential and a linear term modified by a logarithm [46]. To understand the parton deconfinement at finite temperature, we study in this paper the heavy quark potential in the GZ approach at finite temperature in the frame of resummed perturbation theory. We will focus on the region around the deconfinement temperature T_c ($T \leq 2T_c$) which can be realized in high-energy nuclear collisions and where the normal perturbation theories like HTL are not suitable. Since the heavy quark potential is characterized by the gluon propagator, the restriction on gluon field configurations in the GZ approach is thus expected to considerably affect the real and imaginary parts of the potential. We calculate firstly the gluon loop, then the gluon propagator in terms of the resummation of gluon and quark loops, and finally the heavy quark potential through constructing the real-time Wilson loop. We summarize in the end.

The Gribov mass parameter m_G is not a free parameter of the theory. It is a dynamical quantity, being determined in a self-consistent way through a gap equation by minimizing the vacuum energy of the system. At the lowest level, it can be derived from the contribution of a closed loop to the gluon self-energy. In Coulomb gauge, it reads [39]

$$\sum_{n,\boldsymbol{p}} \frac{1}{(-\omega_n^2 + \boldsymbol{p}^2)\boldsymbol{p}^2 + m_G^4} = \frac{3}{2N_c g^2}, \tag{2}$$

where $g(T)$ as a function of temperature is the QCD running coupling constant, N_c the number of color degrees of freedom, and $\sum_{n,\boldsymbol{p}} = T\int d^3\boldsymbol{p}/(2\pi)^3 \sum_n$ includes a summation over the Matsubara frequency $\omega_n = 2n\pi T$ and a three-momentum integration. By evaluating the frequency summation, the gap equation is simplified as

$$\int \frac{d^3\boldsymbol{p}}{(2\pi)^3}\frac{1}{\epsilon_p \boldsymbol{p}^2}\left(1 + \frac{2}{e^{\epsilon_p/T} - 1}\right) = \frac{3}{N_c g^2}, \tag{3}$$

where $\epsilon_p = \sqrt{\boldsymbol{p}^2 + m_G^4/\boldsymbol{p}^2}$ can be considered as the effective gluon energy. By making use of the formula

$$\mu^{4-D}\int \frac{d^{D-1}p}{(2\pi)^{D-1}}\frac{D-2}{2\epsilon_p p^2} = \left(\frac{m}{\mu}\right)^{D-4}\frac{D-2}{2(4\pi)^{D/2}}\frac{\Gamma((D-2)/4)\Gamma((4-D)/4)}{\Gamma((D-1)/2)}, \tag{4}$$

we can isolate the divergence in the integration. By taking the standard $\overline{\text{MS}}$ renormalization scheme, the gap equation becomes

$$\frac{1}{4}\ln\left(\frac{e}{2}\frac{\mu^2}{m_G^2}\right) + \int_0^\infty \frac{dx}{u}\frac{1}{e^{m_G u/T} - 1} = \frac{3\pi^2}{N_c g^2(T)}, \tag{5}$$

with $u = \sqrt{x^2 + 1/x^2}$, where μ is the renormalization scale that controls the vacuum value of the Gribov mass.

The temperature dependence of the Gribov mass is characterized by not only the statistical distribution but also the coupling constant $g^2(T) = 4\pi\alpha_s(T)$. At very high temperatures with $T \gtrsim 3T_c$, the IR and UV behaviors of the coupling are obtained through lattice simulations [18], and the results are qualitatively consistent with the perturbative QCD calculation up to two loops [18], as shown in Fig. 1.

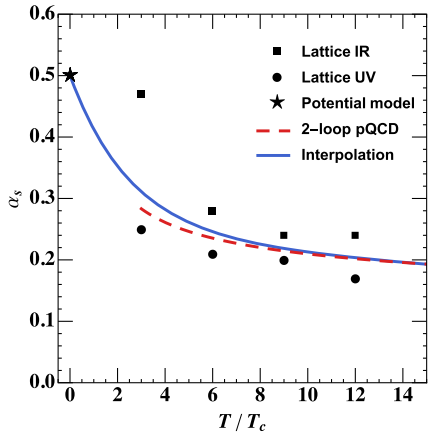

FIG. 1. The running coupling constant $\alpha_s(T)$ calculated by lattice IR and UV [18], perturbative QCD up to two loops [18], potential models [4,24], and interpolation. The deconfinement temperature T_c is chosen to be 170 MeV [24].

In a vacuum the coupling can be extracted by fitting the quarkonium spectra via potential model [4] or fitting the vacuum potential with Cornell potential [23], both give a coupling $\alpha_s \approx 0.5$. For the gap around T_c where charmonium and bottomonium states are expected to be dissociated, which we are interested in for this paper, the nonperturbative effect is strong, and it is hard to find precise calculation. We take an interpolation to continuously connect the vacuum and high-temperature values; see the solid line in Fig. 1.

With the running coupling extracted from the interpolation, we solve the gap equation numerically and obtain the Gribov mass m_G as a function of temperature, shown in Fig. 2. The vacuum value is chosen to be $m_G(0) = 0.55$ GeV, corresponding to the renormalization scale $\mu = 10.92$ GeV in the gap equation. We will see in the following that this value can reproduce the Cornell potential well. The Gribov mass drops down rapidly in the beginning, when the temperature is below the deconfinement temperature, and then becomes smooth in the deconfinement phase. In the limit of high temperature $T \to \infty$, the solution of the gap equation becomes

$$m_G(T) = \frac{N_c}{2^{3/2}3\pi} g^2(T) T \tag{6}$$

and behaves like the standard magnetic mass $m \sim g^2(T)T$ [39,44]. In the asymptotic free interval with $T \to \infty$, $g^2 \sim 1/\ln T$ goes to zero, and the Gribov mass $m_G \sim T/\ln T$ goes to infinity. We think this is not a physical result. The divergent Gribov mass here may come from the running coupling which is calculated in QCD rather than the GZ approach. Considering the self-consistency, we need to calculate both the running coupling and the gap equation in the GZ approach up to order g^2. While this will not remarkably change our result around the phase transition, we will consider the self-consistent calculation in the future.

To include loop correction to the gluon propagator (1), we calculate first the gluon loop. Since the interaction potential between two heavy quarks is only related to the component D_{00} of the gluon propagator $D_{\mu\nu}$, we consider in the following only the component Π_{00} of the loop function $\Pi_{\mu\nu}(p)$. Defining $\Pi_G(p) = -\Pi_{00}(p)/(g^2 N_c \boldsymbol{p}^2)$, a direct calculation leads to

$$\begin{aligned}
\Pi_G(p) &= J_1(p) - J_2(p), \\
J_1(p) &= \sum_{n,\boldsymbol{k}} \frac{3 p_i p_j T^{ij}(\boldsymbol{k})}{(\epsilon_k^2 + \omega_n^2)\boldsymbol{p}^2(\boldsymbol{k}-\boldsymbol{p})^2}, \\
J_2(p) &= \sum_{n,\boldsymbol{k}} \frac{T_{ij}(\boldsymbol{k}) T^{ij}(\boldsymbol{k}-\boldsymbol{p})(\epsilon_k^2 - \omega_n^2 - i\omega_n p_0)}{(\epsilon_k^2 + \omega_n^2)(\epsilon_{k-p}^2 - (i\omega_n - p_0)^2)\boldsymbol{p}^2},
\end{aligned} \tag{7}$$

with $T_{ij}(\boldsymbol{k}) = \delta_{ij} - k_i k_j/\boldsymbol{k}^2$, $i, j = 1, 2, 3$. Similar to the treatment for the gap equation (2), here J_1 and J_2 can be separated into a vacuum part and a thermal part. The latter is convergent, and the former is divergent and needs to be regularized. Introducing a momentum-cutoff Λ and using the renormalization scheme $\overline{\text{MS}}$, the divergence can be attracted into the running coupling,

$$\frac{1}{g^2(\Lambda) N_c} = \frac{1}{48\pi^2}\left(11 \log\frac{\Lambda^2}{\Lambda_{\overline{\text{MS}}}^2} - \frac{49}{3} + 22\log 2\right), \tag{8}$$

where the momentum-cutoff in the scheme $\overline{\text{MS}}$ is taken as $\Lambda_{\overline{\text{MS}}} = m_G/1.62$, including the quark contribution [46].

J_2 can further be separated into three parts:

$$\begin{aligned}
J_2(p) &= J_{2A}(p) + J_{2B}(p) + J_{2C}(p), \\
J_{2A}(p) &= \sum_{n,\boldsymbol{k}} \frac{T_{ij}(\boldsymbol{k}) T^{ij}(\boldsymbol{k}-\boldsymbol{p})}{((i\omega_n - p_0)^2 - \epsilon_{k-p}^2)\boldsymbol{p}^2}, \\
J_{2B}(p) &= \sum_{n,\boldsymbol{k}} \frac{-2\epsilon_k^2 T_{ij}(\boldsymbol{k}) T^{ij}(\boldsymbol{k}-\boldsymbol{p})}{(\omega_n^2 + \epsilon_k^2)((i\omega_n - p_0)^2 - \epsilon_{k-p}^2)\boldsymbol{p}^2}, \\
J_{2C}(p) &= \sum_{n,\boldsymbol{k}} \frac{i\omega_n p_0 T_{ij}(\boldsymbol{k}) T^{ij}(\boldsymbol{k}-\boldsymbol{p})}{(\omega_n^2 + \epsilon_k^2)((i\omega_n - p_0)^2 - \epsilon_{k-p}^2)\boldsymbol{p}^2}.
\end{aligned} \tag{9}$$

Because a statical potential is calculated at time $t \to \infty$ which corresponds to $p_0 \to 0$, J_{2C} disappears in this limit. Taking into account the Matsubara summations,

$$\begin{aligned}
T\sum_n \frac{-1}{\omega_n^2 + \epsilon_k^2} &= -\frac{1}{2\epsilon_k}\coth\frac{\epsilon_k}{2T}, \\
T\sum_n \frac{-1}{(\omega_n^2 + \epsilon_k^2)((i\omega_n - p_0)^2 - \epsilon_{k-p}^2)} &= -\sum_{\eta_1,\eta_2=\pm} \frac{\eta_1\eta_2}{4\epsilon_k\epsilon_{k-p}} \frac{f_B(\eta_2\epsilon_{k-p}) - f_B(\eta_1\epsilon_k)}{p_0 - \eta_1\epsilon_k + \eta_2\epsilon_{k-p}},
\end{aligned} \tag{10}$$

where $f_B(x) = 1/(e^{x/T} - 1)$ is the Bose-Einstein distribution function, J_1 and J_2 can be expressed as

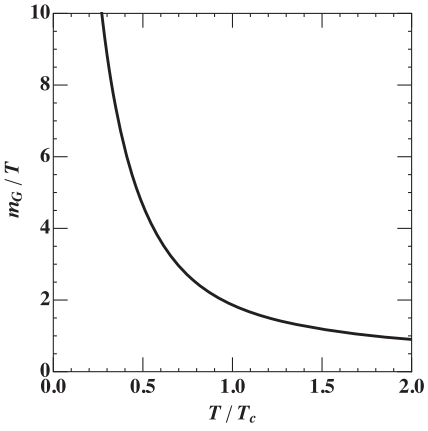

FIG. 2. The Gribov mass $m_G(T)/T$.

$$J_1(p) = \int \frac{d^3\boldsymbol{k}}{(2\pi)^3} \frac{3p_i p_j T^{ij}(\boldsymbol{k})}{2\epsilon_k \boldsymbol{p}^2 (\boldsymbol{k}-\boldsymbol{p})^2} \coth\frac{\epsilon_k}{2T},$$
$$J_{2A}(p) = -\int \frac{d^3\boldsymbol{k}}{(2\pi)^3} \frac{T_{ij}(\boldsymbol{k}) T^{ij}(\boldsymbol{k}+\boldsymbol{p})}{2\epsilon_k \boldsymbol{p}^2} \coth\frac{\epsilon_k}{2T},$$
$$J_{2B}(p) = -\int \frac{d^3\boldsymbol{k}}{(2\pi)^3} \sum_{\eta_1,\eta_2=\pm} \frac{\eta_1\eta_2\epsilon_k T_{ij}(\boldsymbol{k}) T_{ij}(\boldsymbol{k}-\boldsymbol{p})}{2\epsilon_{k-p}\boldsymbol{p}^2} \times \frac{f_B(\eta_2\epsilon_{k-p}) - f_B(\eta_1\epsilon_k)}{p_0 - \eta_1\epsilon_k + \eta_2\epsilon_{k-p}}. \tag{11}$$

We now take an analytic extension of $p_0 \to p_0 + i\epsilon$ which leads to the real and imaginary parts of the gluon loop function,

$$\mathrm{Re}\Pi_G(p) = J_1(p) - J_{2A}(p) - J_{2B}(p),$$
$$\mathrm{Im}\Pi_G(p) = -\pi \int \frac{d^3\boldsymbol{k}}{(2\pi)^3} \sum_{\eta_1\eta_2=\pm} \frac{\eta_1\eta_2\epsilon_k}{2\epsilon_{k-p}\boldsymbol{p}^2} \times [f_B(\eta_2\epsilon_{k-p}) - f_B(\eta_1\epsilon_k)](1+\cos^2\theta) \times \delta(p_0 - \eta_1\epsilon_k + \eta_2\epsilon_{k-p}), \tag{12}$$

where θ is the angle between the two momentum vectors $\boldsymbol{k}$ and $\boldsymbol{k}-\boldsymbol{p}$, and the δ function means the energy conservation during the decay process from one gluon to two gluons.

The Gribov region Ω changes only the path integration of the gauge field, the free quark propagator, and in turn, the quark loop function is not affected by the Gribov condition and can be found in textbooks [47]:

$$\mathrm{Re}\Pi_Q(p) = \frac{N_f}{N_c\boldsymbol{p}^2}\left[\frac{T^2}{12} + \int \frac{d^3\boldsymbol{k}}{(2\pi)^3} \sum_{\eta_1\eta_2=\pm} \eta_1\eta_2 \times \frac{\boldsymbol{k}\cdot(\boldsymbol{k}-\boldsymbol{p})}{|\boldsymbol{k}||\boldsymbol{k}-\boldsymbol{p}|} \frac{f_F(\eta_2|\boldsymbol{k}-\boldsymbol{p}|) - f_F(\eta_1|\boldsymbol{k}|)}{p_0 - \eta_1|\boldsymbol{k}| + \eta_2|\boldsymbol{k}-\boldsymbol{p}|}\right],$$
$$\mathrm{Im}\Pi_Q(p) = -\frac{\pi N_f}{N_c\boldsymbol{p}^2} \int \frac{d^3\boldsymbol{k}}{(2\pi)^3} \sum_{\eta_1\eta_2=\pm} \frac{\eta_1\eta_2\boldsymbol{k}\cdot(\boldsymbol{k}-\boldsymbol{p})}{|\boldsymbol{k}||\boldsymbol{k}-\boldsymbol{p}|} \times [f_F(\eta_2|\boldsymbol{k}-\boldsymbol{p}|) - f_F(\eta_1|\boldsymbol{k}|)] \times \delta(p_0 - \eta_1|\boldsymbol{k}| + \eta_2|\boldsymbol{k}-\boldsymbol{p}|), \tag{13}$$

where $f_F(x) = 1/(e^{x/T}+1)$ is the Fermi-Dirac distribution function. While the quark loop Π_Q is not explicitly affected by the GZ approach, its renormalization in a vacuum is coupled to the Gribov mass m_G through the momentum cutoff $\Lambda_{\overline{\mathrm{MS}}}$.

The total loop function contains both gluon and quark loops,

$$\Pi(p) = \Pi_G(p) + \Pi_Q(p). \tag{14}$$

By summarizing overall gluon and quark loops on a chain [47], one derives the loop-corrected gluon propagator:

$$D_{00}(p) = \frac{1}{\boldsymbol{p}^2}[1 - \Pi_{00}(p)/\boldsymbol{p}^2 + (-\Pi_{00}(p)/\boldsymbol{p}^2)^2 + \cdots] = \frac{1}{\boldsymbol{p}^2}\frac{1}{1 - g^2 N_c \Pi(p)}. \tag{15}$$

We now turn to the calculation of heavy quark potential via the gluon propagator D. Aiming to an in-medium potential, we follow the strategy in Ref. [29] to construct a real-time Wilson loop that characterizes the propagation of two infinitely heavy quarks. The evolution of the Wilson loop satisfies the Schrödinger equation where the potential to the first order of g^2 reads [29]

$$V_>(t,r) = g^2 C_F \int \frac{d^3\boldsymbol{p}}{(2\pi)^3} \frac{2 - e^{ip_3 r} - e^{-ip_3 r}}{2} \times \left\{\frac{1}{\boldsymbol{p}^2(1 - g^2 N_c \Pi(0,\boldsymbol{p}))} + \int \frac{dp_0}{\pi} f_B(p_0) p_0 \times (e^{p_0/T} e^{-ip_0 t} - e^{ip_0 t}) \left[\left(\frac{1}{\boldsymbol{p}^2} - \frac{1}{p_0^2}\right)\rho_E(p) - \left(\frac{1}{\boldsymbol{p}^2} - \frac{1}{p_3^2}\right)\rho_T(p)\right]\right\}, \tag{16}$$

with the constant $C_F = (N_c^2 - 1)/(2N_c)$, where $\rho_E(p)$ and $\rho_T(p)$ are the two spectral functions [29]. Using the relation $\lim_{t\to\infty}(e^{ip_0 t} - e^{-ip_0 t})/p_0 = 2\pi i\delta(p_0)$ and the approximation $f_B(p_0) \approx T/p_0$ for thermalized gluons, we obtain the static potential in the limit of $t \to \infty$:

$$V(r) = \lim_{t\to\infty} V_>(t,r) = V_R(r) + iV_I(r)$$
$$V_R(r) = -\frac{C_F}{N_c}\int \frac{d^3\boldsymbol{p}}{(2\pi)^3} \frac{1}{\boldsymbol{p}^2 \mathrm{Re}\Pi(0,\boldsymbol{p})}(1 - e^{ip_3 r}),$$
$$V_I(r) = \frac{C_F}{N_c} T \int \frac{d^3\boldsymbol{p}}{(2\pi)^3} \frac{\boldsymbol{p}^2 F(0,\boldsymbol{p})}{|\boldsymbol{p}|(\boldsymbol{p}^2 \mathrm{Re}\Pi(0,\boldsymbol{p}))^2}(1 - e^{ip_3 r}) \tag{17}$$

with

$$F(p) = 2\frac{|\boldsymbol{p}|}{p_0}\mathrm{Im}\Pi(p). \tag{18}$$

In a vacuum there is no Landau damping, the imaginary parts of the loop function, propagator, and potential disappear automatically, and the potential is reduced to

$$V(r) = C_F g^2 \int \frac{d^3\boldsymbol{p}}{(2\pi)^3} D_{00}(0,\boldsymbol{p})(1 - e^{i\boldsymbol{p}\cdot\boldsymbol{r}}), \tag{19}$$

which reproduces well the Cornell potential $V(r) = -\alpha/r + \sigma r$ with $\alpha = 0.4105$ and $\sigma = 0.2\ \mathrm{GeV}^2$ [4], see the comparison in Fig. 3.

The heavy quark potential in the medium contains real and imaginary parts, shown in Figs. 4 and 5 at several

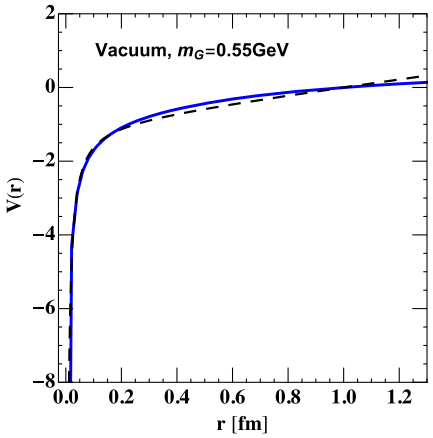

FIG. 3. The vacuum potential $V(r)$ scaled by the condition $V = 0$ at $r = 1$ fm. The dashed and solid lines are calculated via Cornell potential and the Gribov-Zwanziger approach.

temperatures. The real part $V_R(r)$ is, as usually discussed in literature [17], controlled by color screening. In a vacuum, the potential increases linearly with the distance and is never saturated, which means parton confinement. In a hot medium, the long-distance potential is screened, and the screening length decreases with increasing temperature. When the screening length is comparable with a quarkonium radius $r_{Q\bar{Q}}$, the quarkonium starts to be dissociated. This screening picture is widely used to explain the quarkonium suppression observed in high-energy nuclear collisions [17].

Besides the Debye screening, quarkonia will also suffer dynamic dissociation induced by Landau damping and the breakup of a color-singlet bound state into a color-octet heavy quark-antiquark pair by absorption of a thermal gluon. The dissociation processes can effectively be summarized in the imaginary part $V_I(r)$ of the potential. We can see that the imaginary part calculated with the GZ approach keeps zero in a vacuum and increases with the relative distance r at finite temperature. This r-dependence is

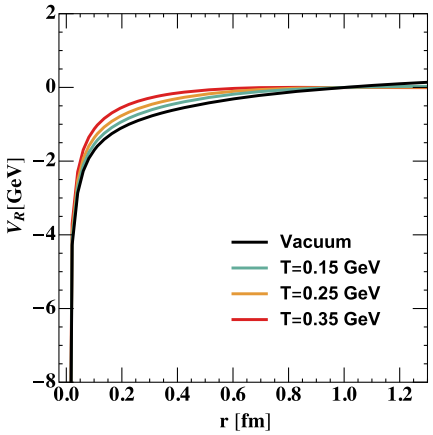

FIG. 4. The real potential $V_R(r)$ at finite temperature, scaled by the condition $V_R = 0$ at $r = 1$ fm.

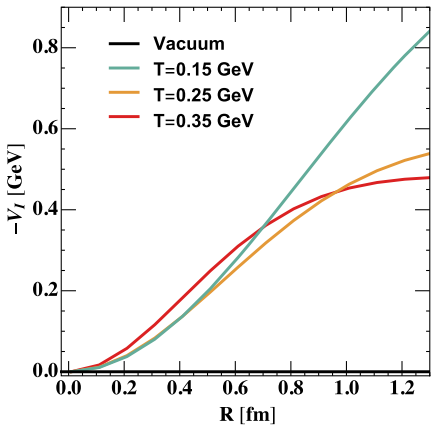

FIG. 5. The imaginary potential $V_I(r)$ at finite temperature.

reasonable because the dissociation becomes easy for large-size quarkonia. Around the phase transition temperature, the strength of V_I is comparable with V_R at $r \sim r_{Q\bar{Q}} \sim 0.5$ fm and much stronger than V_R at $r > r_{Q\bar{Q}}$.

We now compare our results with the ones obtained with lattice simulations and in the HTL approach. For the real potential, our calculation is similar to the lattice data [24] in a wide temperature region, while due to the very large uncertainty in the lattice-simulated imaginary potential [24], it is hard to see the difference between our calculated V_I and the lattice data.

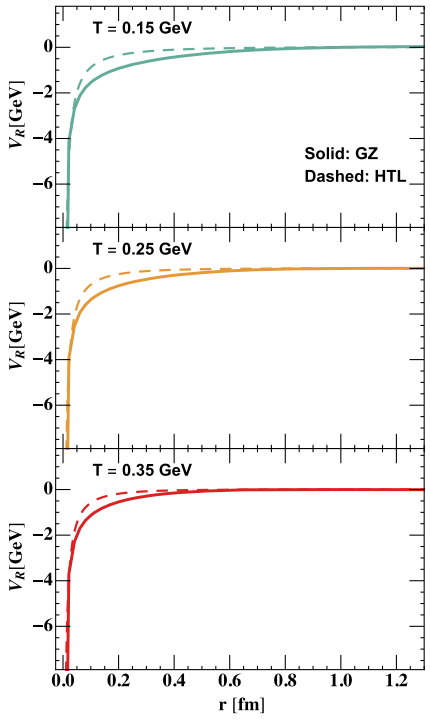

FIG. 6. The comparison of the real potential $V_R(r)$ calculated via the Gribov-Zwanziger (solid lines) and HTL approach (dashed lines).

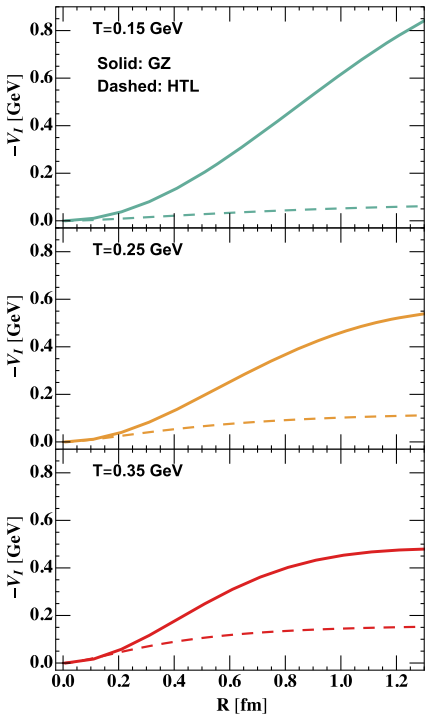

FIG. 7. The comparison of the imaginary potential $V_I(r)$ calculated via the Gribov-Zwanziger (solid lines) and HTL approach (dashed lines).

The heavy quark potential in the HTL approach [29] can be expressed as

$$V(r) = -\frac{C_F g^2}{4\pi}\left[\left(m_D + \frac{e^{-m_D r}}{r}\right) + iT\phi(m_D r)\right],$$
$$\phi(x) = 2\int_0^\infty dz \frac{z}{(z^2+1)^2}\left(1 - \frac{\sin(zx)}{zx}\right), \tag{20}$$

where $m_D = gT\sqrt{N_c/3 + N_f/6}$ is the Debye mass. The real and imaginary potentials calculated in the GZ and HTL approach are compared in Figs. 6 and 7. Firstly, it should be pointed out that it looks not very reasonable to use the HTL approach around the phase transition region since the HTL approach is a good approximation only in high-temperature limits. While the real potentials in the two approaches are close to each other at high temperatures (see Fig. 6), the imaginary part in the GZ approach is much stronger than the one in the HTL approach even at temperature $T = 0.35\ \text{GeV} \sim 2T_c$ (see Fig. 7). The reason is the lack of the magnetic scale in the HTL approach with only one-loop correction. The introduction of the Gribov mass, which is proportional to the magnetic mass, makes our calculation around the phase transition reasonable and leads to the big difference in the imaginary potential between the two approaches.

In summary, we have calculated the loop-corrected heavy quark potential in the Gribov-Zwanziger approach in a strongly coupled quark-gluon plasma. Besides the color screening shown in the real part of the potential, there exists a large imaginary part of the potential, especially around the phase transition temperature, see the upper panel of Fig. 7. We can use the Schrödinger equation to effectively describe the quarkonium decay rate by the imaginary potential [48],

$$\Gamma = 2\int d^3\boldsymbol{x}(-V_I(\boldsymbol{x}))|\psi(\boldsymbol{x})|^2, \tag{21}$$

where ψ is the quarkonium wave function. Since V_I is negative, this decay in the quark-gluon plasma will enhance the quarkonium suppression in high-energy heavy-ion collisions.

The work is supported by the Guangdong Major Project of Basic and Applied Basic Research No. 2020B0301030008 and the NSFC Grants No. 11890712 and No. 12075129.

[1] W. E. Caswell and G. P. Lepage, Phys. Lett. **167B**, 437 (1986).
[2] N. Brambilla, A. Pineda, J. Soto, and A. Vairo, Nucl. Phys. **B566**, 275 (2000).
[3] N. Brambilla, A. Pineda, J. Soto, and A. Vairo, Rev. Mod. Phys. **77**, 1423 (2005).
[4] See for instance the recent review paper, J. Zhao, K. Zhou, S. Chen, and P. Zhuang, Prog. Part. Nucl. Phys. **114**, 103801 (2020).
[5] Y. Koma, M. Koma, and H. Wittig, Phys. Rev. Lett. **97**, 122003 (2006).
[6] T. Kawanai and S. Sasaki, Phys. Rev. D **85**, 091503 (2012).
[7] T. Matsui and H. Satz, Phys. Lett. B **178**, 416 (1986).
[8] X. Dong and V. Greco, Prog. Part. Nucl. Phys. **104**, 97 (2019).
[9] A. Rothkopf, Phys. Rep. **858**, 1 (2020).
[10] E. Chapon, D. d'Enterria, B. Ducloue, M. G. Echevarria, P. B. Gossiaux, V. Kartvelishvili, T. Kasemets, J. P. Lansberg, R. McNulty, D. D. Price *et al.*, Prog. Part. Nucl. Phys. **122**, 103906 (2022).
[11] J. Zhao, S. Shi, and P. Zhuang, Phys. Rev. D **102**, 114001 (2020).
[12] J. Zhao, H. He, and P. Zhuang, Phys. Lett. B **771**, 349 (2017).
[13] H. He, Y. Liu, and P. Zhuang, Phys. Lett. B **746**, 59 (2015).

[14] S. Cho *et al.* (ExHIC Collaboration), Prog. Part. Nucl. Phys. **95**, 279 (2017).
[15] S. Nadkarni, Phys. Rev. D **34**, 3904 (1986).
[16] C. Y. Wong, Phys. Rev. C **72**, 034906 (2005).
[17] H. Satz, J. Phys. G **32**, R25 (2006).
[18] O. Kaczmarek, F. Karsch, F. Zantow, and P. Petreczky, Phys. Rev. D **70**, 074505 (2004); **72**, 059903(E) (2005).
[19] N. Brambilla, J. Ghiglieri, A. Vairo, and P. Petreczky, Phys. Rev. D **78**, 014017 (2008).
[20] A. Bazavov, Y. Burnier, and P. Petreczky, Nucl. Phys. **A932**, 117 (2014).
[21] A. Rothkopf, T. Hatsuda, and S. Sasaki, Phys. Rev. Lett. **108**, 162001 (2012).
[22] Y. Burnier, O. Kaczmarek, and A. Rothkopf, Phys. Rev. Lett. **114**, 082001 (2015).
[23] Y. Burnier, O. Kaczmarek, and A. Rothkopf, J. High Energy Phys. 12 (2015) 101.
[24] D. Lafferty and A. Rothkopf, Phys. Rev. D **101**, 056010 (2020).
[25] D. Bala and S. Datta, Phys. Rev. D **101**, 034507 (2020).
[26] S. Shi, K. Zhou, J. Zhao, S. Mukherjee, and P. Zhuang, Phys. Rev. D **105**, 014017 (2022).
[27] R. Larsen, S. Meinel, S. Mukherjee, and P. Petreczky, Phys. Lett. B **800**, 135119 (2020).
[28] D. Bala *et al.* (HotQCD Collaboration), Phys. Rev. D **105**, 054513 (2022).
[29] M. Laine, O. Philipsen, P. Romatschke, and M. Tassler, J. High Energy Phys. 03 (2007) 054.
[30] A. Beraudo, J. P. Blaizot, and C. Ratti, Nucl. Phys. **A806**, 312 (2008).
[31] A. D. Linde, Phys. Lett. **96B**, 289 (1980).
[32] R. Jackiw and S. Y. Pi, Phys. Lett. B **368**, 131 (1996).
[33] L. D. Faddeev and V. N. Popov, Phys. Lett. B **25**, 29 (1967).
[34] V. N. Gribov, Nucl. Phys. **B139**, 1 (1978).
[35] Y.Dokshitzer and D.Kharzeev, Annu. Rev. Nucl. Part. Sci. **54**, 487 (2004).
[36] D. Zwanziger, Nucl. Phys. **B209**, 336 (1982).
[37] D. Zwanziger, Nucl. Phys. **B323**, 513 (1989).
[38] D. Zwanziger, Nucl. Phys. **B399**, 477 (1993).
[39] D. Zwanziger, Phys. Rev. D **76**, 125014 (2007).
[40] A. Cucchieri and D. Zwanziger, Phys. Rev. D **65**, 014002 (2001).
[41] J. A. Gracey, J. High Energy Phys. 02 (2010) 009.
[42] F. E. Canfora, D. Dudal, I. F. Justo, P. Pais, L. Rosa, and D. Vercauteren, Eur. Phys. J. C **75**, 326 (2015).
[43] See for instance, D. Dudal, O. Oliveira, and P. J. Silva, Ann. Phys. (Amsterdam) **397**, 351 (2018).
[44] K. Fukushima and N. Su, Phys. Rev. D **88**, 076008 (2013).
[45] G. Burgio, M. Quandt, and H. Reinhardt, Phys. Rev. Lett. **102**, 032002 (2009).
[46] M. Golterman, J. Greensite, S. Peris, and A. P. Szczepaniak, Phys. Rev. D **85**, 085016 (2012).
[47] J. I. Kapusta and C. Gale, *Finite-Temperature Field Theory: Principles and Applications* (Cambridge University Press, Cambridge, England, 2009); M. Le Bellac, *Thermal Field Theory* (Cambridge University Press, Cambridge, England, 1996).
[48] J. J. Sakurai, *Modern Quantum Mechanics* (Addison-Wesley Publishing Company, Reading, MA, 1994), Revised ed.